Impact of 3D radiative transfer on airborne NO2 imaging remote sensing over cities with buildings

Marc Schwaerzel et al. 2021

Response to the Reviewer's Comments

We thank the three reviewers for their positive comments, critical assessment and useful points to improve the quality of our paper. In the following we address their concerns point by point. Changes in the paper are shown in blue. We hope we clarified all concerns and that the revised manuscript has improved.

Reviewer 1

Reviewer Point P 1.1 — This paper describes the influence of 3D radiative transfer and shadowing on airborne NO2 retrievals, using a case study over Zurich. The paper is well-organized, concise and easy to follow. I have a couple of general and specific comments. After those are addressed I would recommend it be published in AMT. The study results are interesting but I am not sure how the results can be transferred over to a practical application in retrievals; however, it will be a good reference for the impacts of 3D radiative transfer on these kinds of measurements.

I find the description of the motivation to be unconvincing. The authors point to possible 3D effects as being responsible for the discrepancy between high resolution airborne NO2 maps over urban areas and city-scale urban models, and point to Figure S1 for an example. First, to drive home the need for this study, it would be good to see the motivating figures in the main paper instead of the supplement. To me, the observed and modeled NO2 maps look so very different that I doubt the source of the differences is entirely or even primarily 3D radiative effects. I would suspect issues with the model like inaccuracies in mixed layer height, transport, emissions, and chemistry, or issues with surface reflectance and profile shapes in the retrievals. For instance, there are what look like three plumes in the southwest corner of the map which actually look quite well-represented. Why are these represented fairly well but other plumes are not? It may be that 3D effects are the main reason for observed/model discrepancies, but the current example is unconvincing.

The study's motivation would be more convincing if: 1) The new calculations were actually applied to APEX data to calculate new AMFs, perhaps at the end of the paper, and the new maps showed better agreement with the model or improvements in resolution, or 2) a simulation were done using the GRAL NO2 columns to simulate airborne measurements that use 1D radiative transfer, and these simulations were found to show significant smearing. Even

if this is not possible, I would suggest leaving out the example figure, and be more nuanced in the motivation, i.e., along the lines of "we explore 3D effects as a possible contributor to smearing...". The later results will show whether or not they are significant.

Reply: We agree that difference between the APEX and GRAL NO_2 fields are not only caused 3D radiative transfer effects but also by limitations of the model, which is why it was not added to the main text. The cited conference presentation actually lists some likely necessary model improvements. We have removed the figure from the supplement and instead published the presentation containing the figure on Zenodo (https://doi.org/10.5281/zenodo.5220909). The suggestion to apply the method to APEX data and to compare the map to a GRAMM-GRAL simulation is currently work in progress and will be the topic of future publications. We have revised the introduction keeping a stronger focus on how 3D radiative transfer effects might contribute to spatial smearing and also added a subsection on real application implications:

> A strong indication for the importance of 3D radiative transfer effects is that NO_2 maps obtained from airborne imaging spectrometers over cities are spatially much smoother than one would expect from the instrument resolution and compared to maps obtained from high-resolution city-scale dispersion models, which show, for example, strong gradients in the NO_2 field along major roads (Kuhlmann et al., 2017).

Reviewer Point P 1.2 — My second general comment is that it would be nice to see some discussion of the practical implementation of these calculations. Is it too computationally intensive to use for actual campaign AMF calculations? How would a more realistic albedo field change the results?

Reply: We have added a new section in the paper showing the computation of VCDs from simulated SCDs and discussing the application to real observations as well as challenges (computational costs, realistic albedos and NO_2 fields, etc.):

> The codes developed for this study can also be applied to real observations, for example, to the campaigns conducted with APEX imaging spectrometer. A major challenge is to obtain the required input data. 3D building data are available for many cities, but albedos for ground, roof and walls are generally not available. In addition, realistic 3D NO_2 fields from a building-resolving dispersion model are required to compute the total AMFs, which requires high-resolution emission inventories and additional model development, because most building-resolving models are not optimized for providing realistic vertical distributions of trace gases or cannot not be applied to a full city at high resolution (Berchet et al., 2017).
>
> To minimize 3D effects when using 1D-layer AMFs, it would be recommendable to obtain the airborne spectrometer measurement around local noon when the SZA is lowest and avoid large viewing zenith angles. However, around noon turbulent atmospheric mixing will be strong and the NO_2 distributions would be smoothed as well.
>
> The computation of 3D-box AMFs with buildings is computationally quite expensive, but still manageable for current airborne campaigns. For example, the computation of the 3D-box AMF field for a single

APEX pixel (e.g. on Fig. 6f) takes about 280 s on a single core of our Linux machine (Intel(R) Xeon(R) W-2175 CPU @ 2.50GHz). Processing a full campaign consisting of about 100'000 pixels takes about 23 days using all 14 cores on the system. However, simulating AMFs for an APEX campaign would not require simulation for a 1 km x 1 km domain. Nonetheless, computing 3D-box AMFs is significantly more expensive than computing 1D-layer AMFs and reducing computation time, for example, by finding suitable parametrizations using machine learning, would make it possible to calculate the 3D-box AMFs on smaller hardware, to larger campaigns or to run simulations with more details and at higher spatial resolution.

Reviewer Point P 1.3 — Line 3: It's unlikely that the entire cause would be 3D radiative transfer effects. Should qualify with wording like "3D radiative transfer effects may contribute to this discrepancy due to. . . ."

Reply: Yes you are right that the wording could be misleading. We modified the sentence as following:

This could partly be caused by 3D radiative transfer effects due to observation geometry, adjacency effects and effects of buildings.

Reviewer Point P 1.4 — Line 152: Can you give an estimate (maybe in results section) about how much the results would change for shorter wavelength fitting windows? Shorter wavelengths are used in almost all other airborne and satellite instruments that measure NO2, so this would be most interesting for the majority of readers who do not use APEX data.

Reply: In general shorter wavelength increases scattering and decreases the instrument sensitivity. We simulated the footprint with a wavelength of 420 nm and without buildings to look at sensitivity distribution. It appears that 56% of the sensitivity is located outside the ground pixel. For simulations with buildings this number strongly depends on the buildings locations and the induced shadows and is therefore difficult to generalize. We added the following sentence in the conclusions:

In this study, the simulations were conducted at 490 nm, which corresponds to the center of the fitting window used for NO_2 retrieval from the APEX airborne spectrometer. At shorter wavelength, used by other instruments, scattering increases, which decreases the instrument sensitivity to the main optical path. The footprint simulated with a wavelength of 420 nm (without buildings) shows the increase in scattering and the sensitivity to neighbouring pixels, as 56% of the sensitivity is located outside of the ground pixel.

Reviewer Point P 1.5 — Some mixing of verb tenses in paper. For example, in abstract say "We compute.." then next sentence says "We found. . . "

Reply: We checked verb tenses in the manuscript and fixed the mistakes.

Reviewer Point P 1.6 — Line 63: I'm a bit confused at the wording of this sentence. Should it be "The model, however, is able to . . . "

Reply: We modified the sentence as you suggested.

Reviewer 2

Reviewer Point P 2.1 — This paper looks to address the 3-d radiative transfer effects of urban landscapes on NO2 retrievals. The authors use monte carlo simulations from MYSTIC for a simplified urban landscape in Zurich to examine the impacts of buildings AMF calculations (so called 3D-box AMF). This is a very interesting study with significant implications to airborne retrievals. The only part the authors don't seem to address is how they would account for such 3-d effects in actual airborne retrievals. Many of the assumptions they make in this study would likely not be applicable to real world retrievals. Maybe this will come in a later paper, but it would make the paper stronger to explain how this could be translated into actual retrievals.

Reply: We understand the reviewer's point on the lack of information concerning a real application. We have added a subsection discussing the application to real data. This matter, will be the core of a further study, where we will apply 3D-box AMFs to real APEX data.

> The codes developed for this study can also be applied to real observations, for example, to the campaigns conducted with APEX imaging spectrometer. A major challenge is to obtain the required input data. 3D building data are available for many cities, but albedos for ground, roof and walls are generally not available. In addition, realistic 3D NO_2 fields from a building-resolving dispersion model are required to compute the total AMFs, which requires high-resolution emission inventories and additional model development, because most building-resolving models are not optimized for providing realistic vertical distributions of trace gases or cannot not be applied to a full city at high resolution (Berchet et al., 2017).
>
> To minimize 3D effects when using 1D-layer AMFs, it would be recommendable to obtain the airborne spectrometer measurement around local noon when the SZA is lowest and avoid large viewing zenith angles. However, around noon turbulent atmospheric mixing will be strong and the NO_2 distributions would be smoothed as well.

The computation of 3D-box AMFs with buildings is computationally quite expensive, but still manageable for current airborne campaigns. For example, the computation of the 3D-box AMF field for a single APEX pixel (e.g. on Fig. 6f) takes about 280 s on a single core of our Linux machine (Intel(R) Xeon(R) W-2175 CPU @ 2.50GHz). Processing a full campaign consisting of about 100'000 pixels takes about 23 days using all 14 cores on the system. However, simulating AMFs for an APEX campaign would not require simulation for a 1 km x 1 km domain. Nonetheless, computing 3D-box AMFs is significantly more expensive than computing 1D-layer AMFs and reducing computation time, for example, by finding suitable parametrizations using machine learning, would make it possible to calculate the 3D-box AMFs on smaller hardware, to larger campaigns or to run simulations with more details and at higher spatial resolution.

Reviewer Point P 2.2 — The authors note that 50% of the NO2 sensitivity is from outside the ground pixel for a nadir viewing geometry. They also note that the urban canopy module in MYSTIC currently only supports Lambertian reflections. Could the authors elaborate on how the Lambertian assumption would effect their results? Would it be a safe assumption that accounting for specular reflection you would have less light scattering in from outside the ground pixel?

Reply: The sensitivity to neighboring pixels depends strongly on the reflectance properties of the neighboring pixels. Considering non-Lambertian reflection would increase the complexity of the analysis. If all neighboring pixels are specular reflecting, multiple scattering is required for photons to reach the instrument (except if the direct light path crosses the light-of-sight of the instrument), while only single scattering is required for Lambertian surfaces. As a result, sensitivity would decrease for specular reflection. For real application, surface reflectance would be best described by BRDF functions. We added the following line in the manuscript:

For an even more realistic description of the surface reflectance for real applications, BRDF functions would be a well suited method.

Reviewer Point P 2.3 — The simple assumptions about albedo seem to not be very realistic. It would be nice to do simulations with more reasonable albedos or at least provide some discussion on the possible errors from making these assumptions about the albedo.

Reply: We agree that albedo is important and has a big impact on AMFs. The albedos used in this study were taken from APEX measurements over our study area. While real albedos have some variations, the used values (0.1 and 0.2 for roofs/walls and 0.1 for ground) are typical for this area of the city. However, it is true that albedos can vary for different areas and cities. We added the following paragraph in the conclusions to discuss this in more details:

Generalizing our results to others cities is challenging, because many relevant parameters such as building shapes, surface reflectances and a priori NO_2 distribution vary strongly between different cities. In our

case study, we used a surface reflectance of 0.1, which is a realistic value for Zurich but not necessarily for other cities. In general, a higher surface reflectance of the observed ground pixel implies less atmospheric scattering and a higher sensitivity of the instrument to the main optical path and higher albedo of neighbouring pixels increases the sensitivity to this neighbouring pixel.

Reviewer Point P 2.4 — Pg 1 Ln 18. "by fuel combustion by traffic, heating systems...", suggest changing to "by fuel combustion, traffic, heating systems..."

Reply: We implemented the suggested change.

Reviewer Point P 2.5 — Pg 2 Ln 53. Please spell out MYSTIC completely, the Monte carlo code for the phYSically correct Tracing of photons In Cloud atmospheres

Reply: We spell out MYSTIC completely now.

Reviewer Point P 2.6 — Pg 8 Ln 186 "The reflectance was set to 0.1", please clarify that you are referring to surface reflectance, not top of atmosphere reflectance

Reply: We added "surface" before reflectance.

Reviewer Point P 2.7 — Pg 15, Fig 10 It is curious that the building in the bottom right of the figure shows now shadowing effects despite the sun being to the west. Can you explain why this building is not effect by shadows effects. Even if it was in the shadow of the building to the west, one would still expect and impact on SCDs.

Reply: Excellent observation. We verified the simulation inputs and it appears that the building was missing, because we selected only buildings whose centroids are within the domain, whereas all buildings were included in the drawing of building contours. We run the simulation again including the building. Figure 10 was updated.

Reviewer Point P 2.8 — Pg 15 Line 316 "with 19% and 24% for simulations without aerosols and without and with buildings, respectively". This statement is a bit confusing. I suspect you mean 19% from outside the optical

path with no aerosol/no building and 24% from outside the optical path with no aerosol/with building, but it is not clear

Reply: Yes you are right. We clarified the sentence as following:

> Only a small but not negligible amount of photons are from outside the main optical path, with 19% for a simulation without aerosols and without buildings and 24% for a simulation without aerosols and with buildings.

Reviewer Point P 2.9 — Pg 15 Line 317 should be "The effect becomes more.."

Reply: We corrected the typo.

Reviewer 3

Reviewer Point P 3.1 — The studied 3D effects are indeed a very relevant problem in case of airborne/high resolution spaceborne trace gas retrievals over urban areas. A comment I had on the previous study of Schwaerzel et al., 2020 and also here is that I'm eager to see the impact on the VCD of using 3D BOX-AMFs (with/without building layer) instead of 1D layer-AMFs on a real-world airborne data set. Just as demonstrated with the synthetic data, a sample of an APEX data set acquired over Zurich could be used for this.

Reply: We agree that the application to real observations is important and we are currently in the process to apply 3D-box AMFs to real data from an APEX campaign over Zurich and eventually Munich. However, this step also requires additional work, for example, setting up city-scale dispersion models to have suitable 3D NO_2 fields. Since this additional work would make the manuscript substantially larger, we decided against adding it here.

Reviewer Point P 3.2 — I suggest to add a figure and description where you compute back the VCDs, e.g. based on the SCD-3D (considered that this is the typical smoothed NO2 field observed with an airborne imager) and the AMF-1D. This could demonstrate the impact of smoothing on the retrieved VCD (when compared to the 'true' simulated NO2 field of Fig. 2c) when not considering 3D effects. Same could be done by computing the VCD based on SCD-3D-UC and AMF-3D to demonstrate the impact of adding/neglecting the urban canopy. This would help the interpretation and avoid that a non-careful reader could have the impression that the 3D case leads to a more smoothed NO2 field when looking at the SCDs in Figure 6.

Reply: This is a good suggestion, we added a new section addressing the computation/retrieving of VCDs from (simulated) SCDs that include 3D effects and buildings. We added the following three figures showing VCD fields calculated from the

SCDs calculated with 3D-box AMFs with buildings. Additionally we added a figure showing the VCDs retrived from SCDs calculated with 3D-box AMFs without buildings to the supplement. Figure 1 compares VCDs calculated from the new assumed "true" SCD_{3D-UC} combined with AMFs from (left) 3D-box AMFs accounting for buildings (middle) 1D-layer AMFs and (right) 3D-box AMFs ignoring buildings.

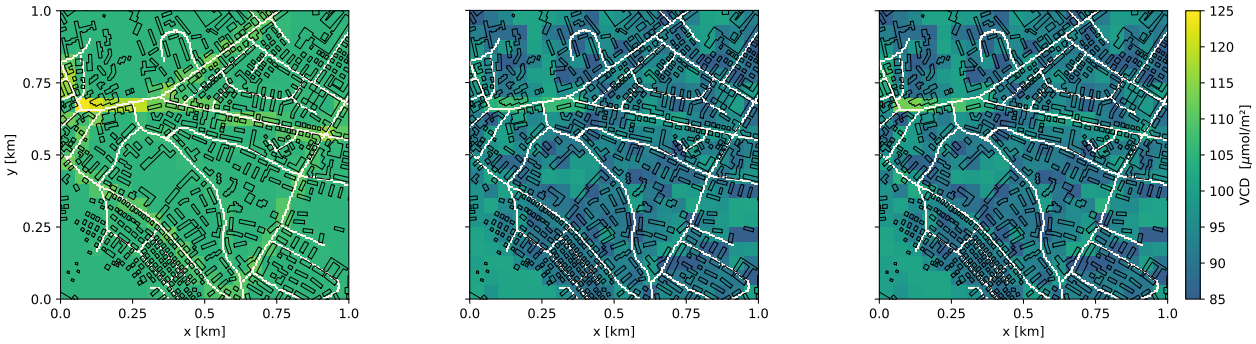

Figure 1. VCDs for a simulation with SAA of 90° with 3D-box AMFs simulation (left) with and (right) without buildings, and with (middle) 1D-layer AMFs.

In the main text we added a subsection containing the following text:

In imaging remote sensing, NO_2 VCDs are retrieved from SCDs using AMFs. Here SCD_{3D-UC} are considered as the "true" SCDs measured by an airborne imaging spectrometer and VCDs were calculated using either 1D-layer AMFs or 3D-box AMFs without buildings (Fig. 11). The VCDs computed with 1D-layer AMFs fails to correct for the spatial smoothing induced by the complex 3D optical path of the photons (Fig. 11b). In additions, the effects of buildings are not corrected resulting in additional noise introduced by shielding effect of the buildings and significantly lower VCDs with a field average of 90.1 µmol m^{-2} compared to the 108.4 µmol m^{-2} of the true VCDs. When VCDs are computed using 3D-box AMFs without buildings, the spatial smearing is corrected but the noise component and lower VCDs (mean: 91.4 µmol m^{-2}) would remain in the retrieved VCDs.

Reviewer Point P 3.3 — This work is building further on an earlier work, i.e. Schwaerzel et al.(2020), and there is clearly an overlap. Please add here explicitly in which way this new study differentiates from the previous study. The full study is not only focusing on the addition of the urban canopy.

Reply: We clarified this point adding the following sentence:

The study builds on the work by Schwaerzel et al. (2020), where we highlighted the importance of 3D RT effects on trace gas remote sensing for ground-based and airborne instruments.

Reviewer Point P 3.4 — Although each building surface can have its own albedo, for reasons of simplicity everything is given the same albedo of 0.1 in the study discussed in 3.3. It is somewhat confusing as sometimes "building shadows" are mentioned in the discussion (pointing to a different albedo). However, I think the authors refer with 'building shadows" rather to areas of the surface that cannot be 'seen'or are 'shielded' due to building obstruction of the lightpath. If this is the case, I would suggest to be more careful with the use of "shadows"or "shadowing effects" in the further discussion and maybe mention it as a 'shielding' effect. I also would explicitly repeat the made assumptions on the albedo in Sect. 3.3.

Reply: The presence of building shadows does not change the albedo of a surface, because the albedo is a property independent of illumination conditions. We have used the term "building shadowing" where the ground pixel is located in the building shadow and, therefore, the direct optical path towards the sun is shielded by the building. However, we noticed that the term "shadowing" is used in BRDF products to describe ground pixels where objects cast shadows. Since this can lead to confusion, we have replaced the term "building shadowing" with "building shielding" in the manuscript.

Reviewer Point P 3.5 — Title: "Cities with buildings"sounds a bit weird. Maybe replace by "built-up areas"?

Reply: We understand your point, as we had the same discussions on the title internally but decided on using "cities with buildings" because it emphasises that buildings have not yet been taken into account in airborne NO_2 remote sensing.

Reviewer Point P 3.6 — p.2, l.28: You might consider adding the following reference : Vlemmix, T., Ge, X. (., de Goeij, B. T. G., van der Wal, L. F., Otter, G. C. J., Stammes, P., Wang, P., Merlaud, A., Schüttemeyer, D., Meier, A. C., Veefkind, J. P., and Levelt, P. F.: Retrieval of tropospheric NO2 columns over Berlin from high-resolution airborne observations with the spectrolite breadboard instrument, Atmos. Meas. Tech. Discuss. [preprint], https://doi.org/10.5194/amt-2017-257, in review, 2017.

Reply: We added the citation.

Reviewer Point P 3.7 — -p.4, l.105: Not clear what the difference is between 'material' and 'material type'. Please specify

Reply: We have rewritten the description of the NetCDF file as follows:

> The triangular mesh is stored in a NetCDF file readable by MYSTIC. An example file layout is shown in the supplement. The file contains the variable `vertices` (shape: $N_v \times 3$, type: double), which is a

list of x, y and z coordinates. A mesh of N_t triangles is build from these vertices using the `triangles` variable (shape: $N_t \times 3$, type: int) by storing the indices of the 3 vertices that create the triangles. The variable `materials_of_triangles` (shape: N_t, type: int) is used to assign each triangle the index of a material type. The material types are defined using the variables `material_type` (shape: N_m, type: string), `material_albedo` (shape: N_m, type: double) and `temperature_of_triangle` (shape: N_m, type: double) to assign a name, albedo and temperature to each material.

Reviewer Point P 3.8 — p.5, l.125: Albedo typically has a strong impact on the AMF. Since the focus of this study is on adding the urban canopy (and its impact), it would be useful for further studies to do a sensitivity test to show the impact on the AMF of different typical roof types (even if the focus of the study here is not specifically on the building albedo).

Reply: We agree that conducting sensitivity studies for varying roof albedos (and other parameters) would be interesting further studies. We partially showed the effect magnitude of a different type of albedo in the supplement for a roof albedo of 0.2. However, we would like to keep the examples simple here to introduce the general concept and leave detailed sensitivity studies for later work.

Reviewer Point P 3.9 — p.7, l.155: I assume this is done for each along-track pixel?

Reply: Yes, each along-track pixel is an average of 10 discrete steps of 5 m (i.e. 10 instrument positions).

Reviewer Point P 3.10 — p.9, l.205: "The slight increase in the column AMFs in the right is induced by scattering events in the right side of the domain appearing on the left of the domain due to circular boundaries"This effect is not well understood.

Reply: Since MYSTIC uses circular boundary conditions, photons leaving the model domain on the left will enter the domain on the right. As a result, column AMFs on the right side of the ground pixel can be increased when the main optical passes overhead in the upper atmosphere for small domains and large SZAs. This model artefact was visible in an early version of the figure. In the current version the artefact cannot be seen anymore, because we only integrate up to 0.4 km. We removed the sentence in the revised version to avoid confusion.

Reviewer Point P 3.11 — p.11, l.251: AMFs calculated with 3D-box AMFs but without buildings (Figure 6b) are lower over the roads and slightly larger just aside the roads." -> it would help the reader to repeat why this is the case.

Reply: We extended the sentence with the following:

> , because the 3D-optical path crosses neighbouring columns with decreased or increased concentrations, respectively.

Reviewer Point P 3.12 — p.12, l. 268: "Not including the urban canopy would therefore underestimate VCDs by 12%..."I first thought to elaborate a bit on this in the conclusion. However, I think it is difficult to generalize, depending on the complexity of the urban canopy and also due to the fact that the bulk of the NO2 can be in elevated layers in real-world conditions which would reduce the impact of adding the UC.

Reply: We agree that a generalisation is difficult because it depends on various factors (urban canopy structure, reflectances, 3D NO_2 distribution). We briefly discuss the limitation of our scenario in the conclusions.

> Generalizing our results to others cities is challenging, because many relevant parameters such as building shapes, surface reflectances and a priori NO_2 distribution vary strongly between different cities. In our case study, we used a surface reflectance of 0.1, which is a realistic value for Zurich but not necessarily for other cities. In general, a higher surface reflectance of the observed ground pixel implies less atmospheric scattering and a higher sensitivity of the instrument to the main optical path and higher albedo of neighbouring pixels increases the sensitivity to this neighbouring pixel.

Reviewer Point P 3.13 — p.15, 322: "When buildings are included, NO2 SCDs are generally lower due to the shadows of building" As you assume a same surface reflectance in the study I assume this is rather due to the blocking of the lighpath?

Reply: Yes (see our reply to point 3.4).

Reviewer Point P 3.14 — Conclusions: Some suggestions would be helpful for future airborne/spaceborne missions and/or instrument design to reduce 3D effects over urban areas, e.g. to operate close to local noon and maybe operate with small VZA, or to put some thresholds on SZA and VZA? The latter is of course a trade-off with the amount of data than can be acquired during an overpass.

Reply: Yes, this is a relevant point. We added a new section 3.4 where we discuss application to real observations and give some recommendations for future campaigns.

The codes developed for this study can also be applied to real observations, for example, to the campaigns conducted with APEX imaging spectrometer. A major challenge is to obtain the required input data. 3D building data are available for many cities, but albedos for ground, roof and walls are generally not available. In addition, realistic 3D NO_2 fields from a building-resolving dispersion model are required to compute the total AMFs, which requires high-resolution emission inventories and additional model development, because most building-resolving models are not optimized for providing realistic vertical distributions of trace gases or cannot not be applied to a full city at high resolution (Berchet et al., 2017).

To minimize 3D effects when using 1D-layer AMFs, it would be recommendable to obtain the airborne spectrometer measurement around local noon when the SZA is lowest and avoid large viewing zenith angles. However, around noon turbulent atmospheric mixing will be strong and the NO_2 distributions would be smoothed as well.

Reviewer Point P 3.15 — p.2, l.31: to -> towards the instrument-

Reply: We corrected this point.

Reviewer Point P 3.16 — p.2,l.40: is NO2 maps -> is that NO2 maps-

Reply: We corrected this point.

Reviewer Point P 3.17 — p.7,l.180: Fig.2c -> Fig. 2c

Reply: We corrected this point.

Reviewer Point P 3.18 — p.7,l.180: Fig.2c -> Fig. 2c (Note as well that references to figures are not always consistent throughout the manuscript. Sometimes written as Figure 1, sometimes as Fig. 1)

Reply: Thank you, we replaced all "Figure" located in the middle of a sentence by "Fig." as required by the AMT style guideline.

Reviewer Point P 3.19 — -p.15, 314: in the direction of -p.16, 326: Two times “have”

Reply: We corrected these mistake.

Reviewer Point P 3.20 — -Fig. 8: This caption is not self-explanatory. Also in the text the figure is not clearly explained.

Reply: We clarified the reference to the figure in the text and modified the caption as following:

Sketch of two main optical paths for an airborne spectrometer pointing at (1) a road in grey and (2) at a pixel aside the road.

Reviewer Point P 3.21 — -Please have a close look at the supplement to correct for typos, e.g. p.2, l. 55: should be 'emission'; add space between 15 and [;'this'parameters 'these'parameters, etc

Reply: We have revised the language and grammar in the supplement and changed "immission" to "concentration" as we refer to a measurable concentration and emissions here.

References

Berchet, A., Zink, K., Muller, C., Oettl, D., Brunner, J., Emmenegger, L., and Brunner, D.: A cost-effective method for simulating city-wide air flow and pollutant dispersion at building resolving scale, Atmospheric Environment, 158, 181–196, https://doi.org/https://doi.org/10.1016/j.atmosenv.2017.03.030, 2017.

Kuhlmann, G., Berchet, A., and Brunner, D.: High-resolution remote sensing and modelling of NO2 air pollution over the city of Zurich, in: 10th EARSeL SIG Imaging Spectroscopy Workshop 2017, Zurich, Switzerland, https://doi.org/10.5281/zenodo.5220909, 2017.

Schwaerzel, M., Emde, C., Brunner, D., Morales, R., Wagner, T., Berne, A., Buchmann, B., and Kuhlmann, G.: Three-dimensional radiative transfer effects on airborne and ground-based trace gas remote sensing, Atmospheric Measurement Techniques, 13, 4277–4293, https://doi.org/https://doi.org/10.5194/amt-13-4277-2020, 2020.

Impact of 3D radiative transfer on airborne NO_2 imaging remote sensing over cities with buildings

Marc Schwaerzel[1,2], Dominik Brunner[1], Fabian Jakub[3], Claudia Emde[3,4], Brigitte Buchmann[1], Alexis Berne[2], and Gerrit Kuhlmann[1]

[1]Empa, Swiss Federal Laboratories for Materials Science and Technology, Dübendorf, Switzerland
[2]Environmental Remote Sensing Laboratory, École Polytechnique Fédérale de Lausanne, Lausanne, Switzerland
[3]Meteorological Institute, Ludwig Maximilian University of Munich, Munich, Germany
[4]German Aerospace Center (DLR), Oberpfaffenhofen, Germany

Correspondence: Gerrit Kuhlmann (gerrit.kuhlmann@empa.ch)

Abstract. Airborne imaging remote sensing is increasingly used to map the spatial distribution of nitrogen dioxide (NO_2) in cities. Despite the small ground-pixel size of the sensors, the measured NO_2 distributions are much smoother than one would expect from high-resolution model simulations of NO_2 over cities. This could partly be caused by 3D radiative transfer effects due to observation geometry, adjacency effects and effects of buildings. Here, we present a case study of imaging a synthetic NO_2 distribution for a district of Zurich using the 3D MYSTIC solver of the libRadtran radiative transfer library. We ~~compute~~ computed NO_2 slant column densities (SCD) using the recently implemented 3D-box air mass factors (3D-box AMF) and a new urban canopy module to account for the effects of buildings. We found that for a single ground pixel (50 m x 50 m) more than 50% of the sensitivity is located outside of the pixel, primarily in the direction of the main optical path between sun, ground pixel, and instrument. Consequently, NO_2 SCDs are spatially smoothed, which results in an increase over roads when they are parallel to the optical path and a decrease otherwise. When buildings are included, NO_2 SCDs are reduced on average by 5% due to the reduced sensitivity to NO_2 in the shadows of the buildings. The effects of buildings also introduce a complex pattern of variability in SCDs that would show up in airborne observations as an additional noise component (about 12 $\mu mol\,m^{-2}$) similar to the magnitude of typical measurement uncertainties. The smearing of the SCDs cannot be corrected using 1D-layer AMFs that assume horizontal homogeneity and thus remains in the final NO_2 map. 3D radiative transfer effects by including buildings need to be considered to compute more accurate AMFs and to reduce biases in NO_2 vertical columns obtained from high-resolution city-scale NO_2 remote sensing.

1 Introduction

Nitrogen oxides (NO_x = NO + NO_2) are key air pollutants mainly emitted by fuel combustion~~by~~, traffic, heating systems, industrial facilities and power plants. Their short lifetime and localized sources result in a high spatial and temporal variability especially in urban areas (Berchet et al., 2017). An attractive possibility to create high-resolution maps (<100 m) of the NO_2 distribution in cities is to use an airborne imaging spectrometer. This was first demonstrated for measurements from the Airborne Prism Experiment (APEX) of a Swiss-Belgium consortium (Popp et al., 2012; Tack et al., 2017) and the Geostationary

Trace gas and Aerosol Sensor Optimization (GeoTASO) spectrometer (Nowlan et al., 2016) developed in the United States. A comprehensive comparison between four airborne NO_2 imaging spectrometers flown over the city of Berlin was performed during the AROMAPEX campaign (Tack et al., 2019), which included APEX (Schaepman et al., 2015), AirMAP (Airborne imaging DOAS instrument for Measurements of Atmospheric Pollution) (Schönhardt et al., 2015), SWING (Small Whiskbroom Imager for atmospheric compositioN monitorinG) (Merlaud et al., 2013) and SBI (Spectrolite Breadboard Instrument) ~~(de Goeij et al., 2017)~~(de Goeij et al., 2017; Vlemmix et al., 2017).

Airborne imaging spectrometers are passive remote sensing instruments from which we can retrieve NO_2 slant column densities (SCD) from backscattered solar radiance spectra. SCDs are defined as the integrated trace gas concentrations along the optical path from the sun, through the atmosphere and ~~to~~ towards the instrument. The optical path and therefore the SCD depends on illumination conditions, viewing geometry, the scattering and absorption by air molecules, aerosols and clouds as well as the reflectance of the surface. To obtain a quantity that is independent of illumination and viewing conditions, SCDs are divided by air mass factors (AMF) to compute vertical column densities (VCD) defined as the vertically integrated concentrations from the ground to the top of the atmosphere.

NO_2 retrieval algorithms applied to airborne instruments have been derived from algorithms developed for satellite instruments with much lower spatial resolution (> 5 km). These algorithms rely on 1D radiative transfer simulations, which reach their limits at high resolution and in the presence of spatially variable properties of the atmosphere and the surface, as they assume horizontal homogeneity of all parameters within the optical path. A strong indication for the importance of 3D radiative transfer effects is that NO_2 maps obtained from airborne imaging spectrometers over cities are spatially much smoother than one would expect from the instrument resolution and compared to maps obtained from high-resolution city-scale dispersion models~~(see smeared NO_2 concentrations in Figure S1 in the supplement taken from Kuhlmann et al., 2017)~~, which show, for example, strong gradients in the NO_2 field along major roads (Kuhlmann et al., 2017). A likely explanation is that the measurements are not only sensitive to NO_2 in the vertical column above the observed ground pixels but also to the atmosphere surrounding the pixels, which is known as the horizontal smoothing error or the adjacency effect (Cracknell and Varotsos, 2012; Lyapustin and Kaufman, 2001; Richter, 1990). The adjacency effect has been described especially in the context of high-resolution land-surface remote sensing, but it has also been discussed in the context of atmospheric measurements (e.g., Richter, 1990; Minomura et al., 2001; de Graaf et al., 2016). Evidence for 3D radiation effects due to the presence of clouds in the vicinity of an observed ground pixel has recently been reported for CO_2 observations from the OCO-2 satellite (Massie et al., 2017). Such effects are expected to become increasingly important with the increasing resolution of satellite observations (Schwaerzel et al., 2020). An additional complexity over cities to be accounted for is the effects of buildings on the photon paths due to multiple reflections and ~~shadowing~~shielding of the main optical path.

The aim of this study is to quantify, for the first time, the impact of these 3D radiative transfer (RT) effects in the presence of spatially variable surface properties and NO_2 concentrations over cities on NO_2 retrievals from high-resolution airborne imaging spectrometers. ~~For this purpose, we use the~~ The study builds on the work by Schwaerzel et al. (2020), where we highlighted the importance of 3D RT effects on trace gas remote sensing for ground-based and airborne instruments. In this study, we also use the Monte carlo code for the phYSically correct Tracing of photons In Cloudy atmospheres (MYSTIC)

solver of the library for Radiative transfer (libRadtran), which is a Monte Carlo solver that traces individual photons in a 3D model grid (Mayer, 2009; Emde and Mayer, 2007). These photon paths are converted to 3D-box AMFs that describe the sensitivity of an instrument to a trace gas (here NO_2) in each grid box (Schwaerzel et al., 2020). To account for the effect of buildings, we additionally implemented a new urban canopy feature that represents the full 3D building structure of a city with assigned optical properties of the different surfaces. 3D radiative transfer calculations in the urban canopy are not new, but so far focused only on applications not related to trace gas observations such as the computation of radiation budgets and broadband landscape imaging (Gastellu-Etchegorry et al., 2015). The present study is the first to use such a model to investigate 3D effects on trace gas retrievals over a city. In order to isolate different effects on 3D-box AMFs and on the spatial smoothing of the information retrieved from an airborne instrument, we use a comparatively simple setup with 3D buildings representative of a district in the city of Zurich with uniform optical properties of roofs, walls and streets. The model, however, ~~would be~~ is able to describe the optical properties of each single surface separately.

2 Methods

2.1 The MYSTIC radiative transfer solver

~~The MYSTIC radiative transfer (RT)~~ MYSTIC is operated as a RT solver of the libRadtran package ((Mayer and Kylling, 2005; Emde et al., . The MYSTIC RT solver is based on the Monte Carlo principle to calculate different radiative quantities such as irradiance, radiance, absorption, emission, actinic flux, photon's path length and air mass factors (Mayer, 2009; Emde and Mayer, 2007; Schwaerzel et al., 2020). A Monte Carlo based RTM traces individual photons from the source (e.g., sun) to the instrument (e.g., airborne spectrometer) accounting for ground and atmospheric interactions. Photon paths are treated as a combination of random decisions with a given probability distribution for each interaction (e.g., probability distribution of the scattering direction)~~(Mayer, 2009; Emde and Mayer, 2007; Deutschmann et al., 2011)~~. By tracing several thousands of photons, the averaged photon paths reaching the instrument become representative of the actual photon paths in the atmosphere. To simulate ~~radiative transfer quantities~~ RT quantities such as 3D-box AMFs, photons are traced backwards from the instrument to the sun, which is equivalent to the forward mode but greatly enhances computational efficiency (Marchuk et al., 1980; Emde and Mayer, 2007). MYSTIC divides the atmosphere into 1D vertical layers or 3D grid boxes with different properties and saves the mean photon path length within each layer or box. A plane parallel geometry is used for 3D AMF calculations, while spherical geometry is possible for 1D calculations.

2.1.1 Air mass factors

AMFs are obtained by dividing the mean photon path length in each layer or box by its height. For a layer or box i with given concentration c_i and optical properties, the 1D-layer or 3D-box AMF is given by

$$AMF_i = \frac{SCD_i}{VCD_i} = \frac{\int_{path} c_i dl}{\int_{z_i}^{z_{i+1}} c_i dz} = \frac{\int_{path} dl}{h_i} = \frac{L_i}{h_i} \quad (1)$$

where L_i is the mean optical path in the layer/box i of all photons that reach the instrument and h_i is the height of the layer/box i.

To calculate a total AMF that can be used to convert measured SCDs to VCDs, an a priori VCD (VCD_i) is needed for every layer/box i. For the 1D case, the total AMF is computed as

$$AMF = \frac{\sum_{k=1}^{n_z} AMF_k VCD_k}{\sum_{k=1}^{n_z} VCD_k} = \frac{\sum_{k=1}^{n_z} SCD_k}{\sum_{k=1}^{n_z} VCD_k} \tag{2}$$

where n_z is the number of vertical layers. For the 3D case, the total AMF is computed as

$$AMF = \frac{\sum_{i=1}^{n_x}\sum_{j=1}^{n_y}\sum_{k=1}^{n_z} AMF_{i,j,k} VCD_{i,j,k}}{\sum_{k=1}^{n_z} VCD_k} = \frac{\sum_{i=1}^{n_x}\sum_{j=1}^{n_y}\sum_{k=1}^{n_z} SCD_{i,j,k}}{\sum_{k=1}^{n_z} VCD_k} \tag{3}$$

where n_x and n_y are the number of grid cells in x and y direction. In the 1D case, the AMF depends on the shape of the vertical profile of the trace gas (but not on its abundance) (Palmer et al., 2001). In the 3D case, it additionally depends on the horizontal distribution of the trace gas.

2.1.2 Urban canopy implementation

The urban canopy was implemented in libRadtran as a triangle mesh, where each triangle can be assigned different optical and physical properties. Information on vertex positions and optical properties are read from an input file that has to be generated from a 3D building data set prior to the simulation. Using a ray tracing algorithm newly integrated into the model, MYSTIC detects if and where a photon hits a triangle. The interaction of the photon with the surface (absorption or reflection) is then simulated using preexisting MYSTIC functions.

To create a triangular mesh for each building, a Python script was written that converts buildings stored in an ESRI shapefile into triangles. A building consists of one or several flat roofs and several vertical walls. To create triangles for the roof, we connect the polygon centroid to each polygon corner. Wall triangles are created by splitting each wall diagonally into two triangles. Each triangle surface carries information about its albedo and skin temperature. The skin temperatures are used for thermal simulations, a feature that is not used in this publication. The triangular mesh is stored in a NetCDF file ~~that can be read in by MYSTIC(see an example file in the Supplement)~~readable by MYSTIC. An example file layout is shown in the supplement. The file contains the variable `vertices` (shape: $N_v \times 3$, type: double), which is a list of ~~vertices (list of~~ x, y and z coordinates~~), a list of triangles (index of~~. A mesh of N_t triangles is build from these vertices using the `triangles` variable (shape: $N_t \times 3$, type: int) by storing the indices of the 3 vertices ~~for each triangle), a list of materials (each triangle gets assigned a material), a list of material albedo values, a list of material types (name of materials)and~~ that create the triangles. The variable `materials_of_triangles` (shape: N_t, type: int) is used to assign each triangle the index of a ~~list of materialtemperatures~~material type. The material types are defined using the variables `material_type` (shape: N_m, type: string), `material_albedo` (shape: N_m, type: double) and `temperature_of_triangle` (shape: N_m, type: double) to assign a name, albedo and temperature to each material.

In MYSTIC, each photon is traced step-wise along its optical path from one interaction to the other. To interact with the urban canopy, a ray tracing code searches for hits with one of the triangles during each step. We use the Star-3D li-

brary (https://gitlab.com/meso-star/star-3d) (Villefranque et al., 2019), which is a convenient wrapper for Intel® Embree (www.embree.org) to facilitate efficient ray / triangle intersection tests using a bounding volume hierarchy (BVH).

In the case that a ray hits a surface, a Lambertian reflection happens and a new direction is attributed to the photon, which will continue its path until its next interaction. Absorption on surfaces is accounted for by reducing a photon weight by $1 - albedo$. Currently, the urban canopy module only supports Lambertian reflections but an extension, e.g., to specular reflections would be straightforward. For an even more realistic description of the surface reflectance for real applications, BRDF functions would be a well suited method.

2.2 Study case in Zurich

To study radiative transfer effects on airborne measurements for a realistic scene, we selected a 1 km x 1 km region in Zurich, Switzerland (see Fig. 1a). The low-rise buildings (10-15 m) with simple geometries are rather typical for Swiss cities. The scene includes roads of different widths and orientations and two open areas without buildings.

2.2.1 Buildings

We used 3D building data from a shape file obtained from the Swiss Federal Office of Topography (swisstopo). Each building is defined as a polygon with x and y-coordinate for the edges and the centroid (Swiss LV03 coordinates system) with a single height. As described above, the data was converted to a triangular mesh and saved to a netCDF file. For simplicity, we either applied albedos of 0.1 for walls (identical to the used ground albedo) and 0.2 for roofs or used the same albedo of 0.1 for all surfaces (albedos chosen after Mussetti et al., 2020). Figure 1b shows the buildings colored by their heights in the selected model domain.

2.2.2 Synthetic NO_2 field

We created a simple but quite realistic 3D NO_2 concentration field based on the traffic emission inventory of the city of Zurich (see Table 1 in Berchet et al., 2017). For this purpose, the road emissions available as line sources were rasterized at 5 m x 5 m spatial resolution and normalized by the maximum value in the rasterized field. The normalized field was then multiplied with a NO_2 concentration of 110 $\mu g\,m^{-3}$, which is a typical high concentration measured next to busy streets in Zurich (Bär, 2016). A background NO_2 concentration of 15 μgm^{-3} was added using a typical low value observed in Zurich (Bär, 2016) (see ~~Supplement~~ supplement for details). The maximum concentration is thus 125 $\mu g\,m^{-3}$ or 2.7 $\mu mol\,m^{-3}$. Finally, we smoothed the concentration field with a Gaussian filter with a standard deviation of 5 m to mimic the effect of turbulent dispersion. The synthetic field of the NO_2 near surface concentrations is shown in ~~Figure~~Fig. 2a binned on a 50 m x 50 m grid, which is the typical resolution of trace gas measurements from an airborne instrument like APEX.

The vertical distribution was modelled as a linear decrease from the surface value to the background value of 0.65 $\mu mol\,m^{-3}$ at 100 m. Above 100 m, all profiles decrease exponentially with altitude with an e-folding vertical length scale of 720 m, which was obtained by fitting a function to a measured vertical profile (see ~~Supplement~~supplement). Figure 2b shows a NO_2

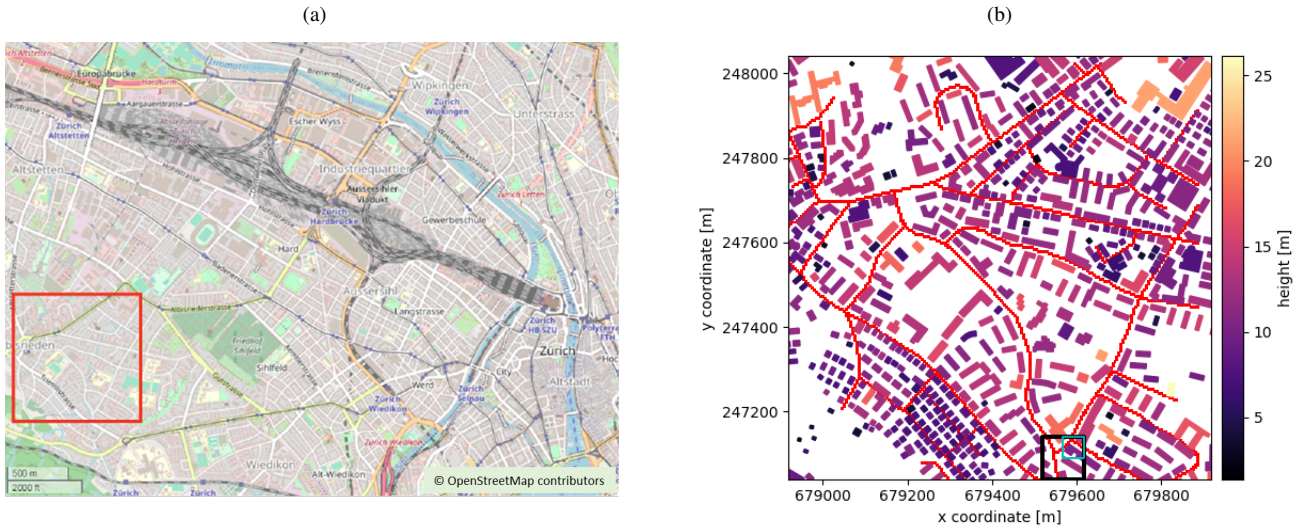

Figure 1. (a) Map of Zurich with the location of the study area in red. Map informations were obtained from OpenStreeMap (© OpenStreetMap contributors 2021. Distributed under the Open Data Commons Open Database License (ODbL) v1.0.) (b) Building heights and major roads in the study area with the lower left pixel at x = 678918 m and y = 247040 m in the Swiss LV03 coordinate system. The black square represents the location of the sub-domain and the cyan square the location of a single pixel observation both used in Section 3.3.

background profile (blue) and a NO_2 profile over the road (red). Figure 2c shows the total VCDs over the selected region in Zurich calculated from the 3D NO_2 concentration field. For more details on the generation of the 3D NO_2 field, please refer to the ~~Supplement~~supplement.

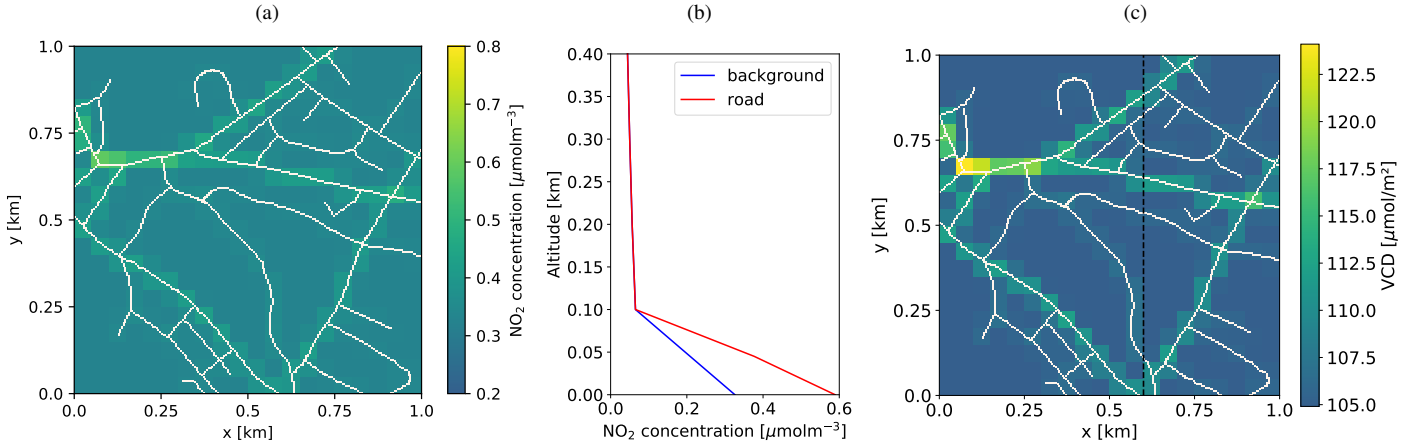

Figure 2. (a) NO_2 ground concentration map. (b) NO_2 vertical profile at a background location (blue line) and over a road at x = 5 m, y = 55 m (red line). (c) Field of vertically integrated NO_2 column densities (VCD) with aircraft flight track overlaid as dashed black line.

2.2.3 MYSTIC simulations

Our scenario corresponds to an airborne imaging spectrometer flying across the model domain from south to north (y-direction) slightly to the east of the center (x=600 m) at an altitude of 6 km, which represents the flight altitude of an airborne spectrometer (dashed black line in Fig. 2c). The viewing zenith angle was varied in discrete steps to cover the whole domain in across-flight direction (i.e. in east-west direction). For simplicity, the sun was placed at an azimuth angle (SAA) of either 90° (i.e. west) or 0° (i.e. south). The solar zenith angle (SZA) was set to 60°, which corresponds to values in the morning or afternoon in summer over Zurich. Simulations with a SZA of 30°, which correspond to typical summer noon measurements over Zurich are shown in the ~~Supplement~~supplement.

The simulations were conducted for a standard atmosphere and for a wavelength of 490 nm, which is the center of the NO_2 fitting window used for the APEX instrument (Kuhlmann et al., 2016). NO_2 absorption features at shorter wavelengths typically used in satellite retrievals are less suitable for APEX due to the high instrument noise at those wavelengths. Note that 3D effects would be stronger at shorter wavelengths due to enhanced Rayleigh scattering. Aerosols were only included in the simulations as a case study to analyse the footprint of the spectrometer (see Sect. 2.3). Table S1 in the ~~Supplement~~ supplement provides an overview of the MYSTIC input parameters used in the simulations.

To resolve the spatial variability of surfaces and elevations within each 50 m x 50 m ground pixel, we specified an instrument opening zenith angle corresponding to the 50 m pixel size in ~~x-direction~~ x-direction and moved the aircraft in 10 discrete steps of 5 m along the ~~y-direction~~y-direction. The 10 different 3D-box AMF fields computed in this way were then averaged to a single field per pixel. The 3D-box AMFs were then used together with the synthetic NO_2 field to compute total SCDs that would be observed from an airborne instrument (see numerator in Eq. 3). ~~Finally~~ Then, the total AMFs were calculated dividing the total SCDs by the total VCDs. In the same way we also computed SCDs ignoring buildings and SCDs based on 1D-layer AMFs (Eq. 2). Differences between the three types of SCDs can be attributed to 3D and building effects. Since in real applications VCDs would be computed from SCDs, we also use the SCD field calculated with 3D-box AMFs including buildings as the "true" SCD measured by the airborne spectrometer and calculate the VCD field using total AMF calculated from 1D-layer AMFs and 3D-box AMFs without considering buildings to show the errors caused by these simplifications.

2.3 Footprint of an airborne spectrometer

To study the sensitivity of a single measurement to the surrounding of the ground pixel, we simulated the horizontal distribution of 3D-box AMFs close to the ground for a single observation scenario. The simulations were conducted without aerosols and for a typical urban aerosol scenario with an aerosol optical depth (AOD) of 0.1. For the scenario, the sensor was placed at x = 675 m and y = 75 m pointing at a ground pixel with the lower left corner located at x = 650 m and y = 50 m. The corresponding VZA was 0.72° in the center of the pixel and the VAA was 270° (instrument pointing eastwards) (for details see also table S1 in the ~~Supplement~~supplement).

To obtain a map of the close-to-ground NO_2 sensitivity of a single ground pixel measured by an airborne imaging spectrometer during a flight overpass, we simulated AMFs with a 5 m x 5 m horizontal resolution and a 5 m vertical resolution in the lowest 45 m above ground for 10 equally-spaced instrument opening zenith angles corresponding to the 50 m pixel size in x-direction and moved the aircraft in 10 discrete steps of 5 m along the y-direction. We averaged the obtained 100 AMFs fields, integrated them vertically for the first 45 m and scaled the result by the sum of all pixels to finally obtain a 2D map of the fraction of the sensitivity within one 5 m x 5 m grid cell. In the following, this will be called the NO_2 footprint of an airborne spectrometer.

3 Results

In this section we first show the instrument incoming radiance calculated with MYSTIC over the selected study area. Second, we analyze the 3D-box AMFs for a single NO_2 observation both in the vertical and in the horizontal and compare results with and without buildings. Finally, we compare total AMFs for the complete image obtained from an airborne instrument flying over the study domain as illustrated in Fig. 2c between the solution obtained with the 3D and the 1D RTM to illustrate the importance of 3D radiative transfer effects on the SCD measurements.

3.1 Incoming radiance

An airborne imaging spectrometer measures radiance from back-scattered and reflected solar irradiance. Figure 3 shows the instrument incoming radiance at 490 nm for the selected region with the urban canopy. Note that for this example the instrument was placed in the center of the domain at an altitude of 6 km observing the scene with a very wide opening angle of about 10° to cover the full 1 km x 1 km domain. The sun is located in the west with a SZA of 60°. The surface reflectance was set to 0.10, while the reflectance of roofs and walls was set to 0.20 in this example.

Since building surfaces have higher reflectance in this example, the bright building roofs clearly stand out. Some bright walls illuminated by the sun can be seen in the east of the domain. Shadows are also clearly visible in the east of the buildings with taller buildings producing longer shadows. This radiance field is closely related to the close-to-ground NO_2 sensitivity. NO_2 over a bright surface can more easily be detected than NO_2 over a dark surface. In case of a pixel covered by both bright and dark surfaces, the retrieved signal will be more strongly affect by NO_2 above the bright parts.

3.2 3D-box air mass factors for a single observation

3.2.1 Vertical distribution along the main optical path

3D-box AMFs have a distinct 3D distribution for each ground pixel. Figure 4a shows an example of the 3D-box AMFs projected onto a 2D (x-z) plane by integrating in y-direction for an instrument pointing almost in nadir direction at the ground pixel centered at x=675 m and y=75 m (~~black square in Figure~~ cyan square in Fig. 1b). Since the pixel is partly covered by buildings, 3D-box AMFs close to the ground (0-10 m) are smaller than those above roof level. Note that in this ~~simulation all surfaces~~

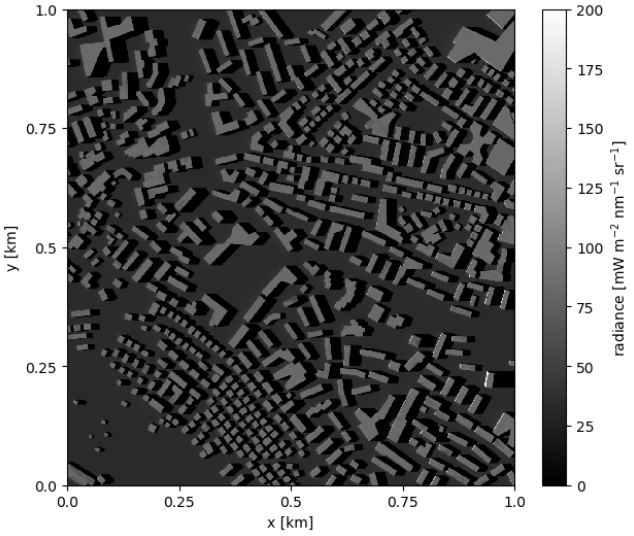

Figure 3. Radiance seen by a downward viewing instrument placed in the center of the 1 km x 1 km region at an altitude of 6 km. SZA and SAA are 60° and 90°, respectively.

~~had~~ and all the following simulations all surfaces have a constant albedo of 0.1. Most photons follow the geometric path from the sun to a reflection on the ground or the roof and to the instrument as indicated by the high 3D-box AMFs along this path. Figure 4b shows the 1D-layer AMFs obtained by integrating the 3D-box AMFs in x- and y-direction. The decrease close to the ground due to the buildings is clearly visible. Figure 4c shows column AMFs along the x-axis, i.e. 3D-box AMFs integrated in y- and z-direction. AMFs in the column directly below the instrument are highest, because the collected photons cross at least one of the column boxes when they are scattered into the direction of the instrument. The column AMFs decrease in the x-direction with distance to the instrument due to atmospheric absorption and scattering. ~~The slight increase in the column AMFs in the right is induced by scattering events in the right side of the domain appearing on the left of the domain due to circular boundaries.~~

Since 3D-box AMFs inform about the sensitivity to NO_2, we can conclude that the measurement is mainly sensitive to NO_2 along the geometrical optical path. It is not very sensitive to adjacent pixels and also not to NO_2 at the surface because of the blocking of the photon path by buildings. The total AMF for the observation presented in this example computed with Eq. 3 is 1.98. The VCD above the ground pixel is 121 $\mu mol\ m^{-2}$ and the SCD computed as VCD times total AMF is 239 $\mu mol\ m^{-2}$.

3.2.2 Horizontal footprint

To further illustrate the horizontal sensitivity of an airborne spectrometer to layers close to the ground, ~~Figure~~ Fig. 5 shows the near-surface footprint defined as the vertically integrated 3D-box AMFs from 0-45 m above ground (see Sect. 2.3). The same scene was simulated as in Section 3.2.1 but with a higher horizontal resolution of 5 m x 5 m to illustrate the spatial pattern of

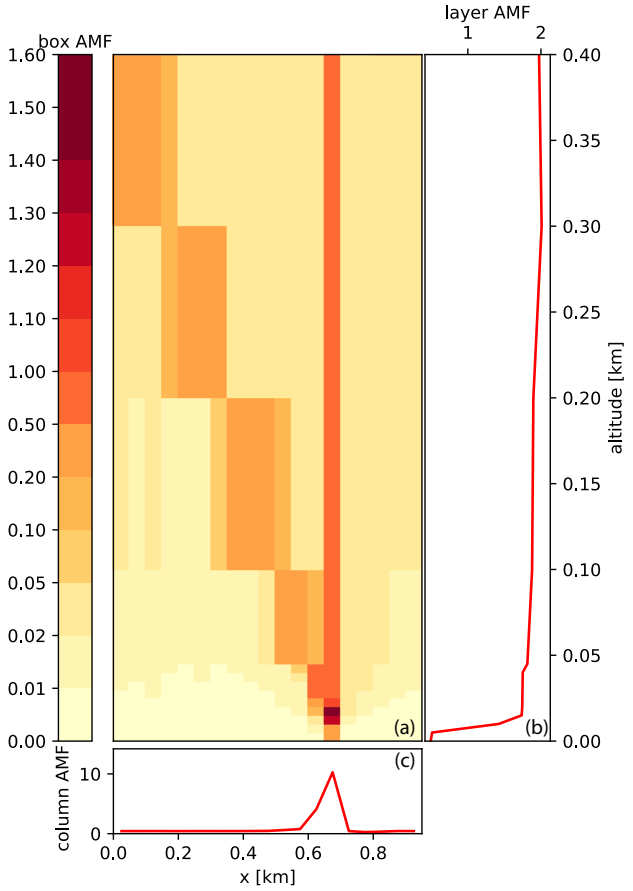

Figure 4. (a) Integrated 3D-box AMFs in y-direction for a ground pixel at x=650 m and y=50 m (lower left corner) for an instrument placed at x=600 m, y=75 m and z=6000 m. The sun is at SAA = 90° (west) with a SZA of 60°. (b) Vertical profile of horizontally integrated AMFs (1D-layer AMFs) and (c) Horizontal profile of vertically integrated AMFs (column AMFs).

the sensitivity in greater detail. The figure is normalized to show the fraction of the sensitivity represented by each 5 m x 5 m pixel.

Figure 5a shows the footprint for a flat surface without buildings without including aerosols. An important part of the sensitivity (51.4%) is located outside the ground pixel. The instrument will thus not only 'see' near-surface NO_2 above the ground pixel but also NO_2 outside. A major part of the sensitivity is located in the direction of the sun along the main optical path. The main optical path is dominated by photons that are either reflected from the ground pixel surface or scattered in the atmosphere above the ground pixel one single time upward into the direction of the instrument. A much smaller fraction is located outside this main path and is caused by photons experiencing at least one more scattering (or reflection) event before being scattered (or reflected) into the main optical path.

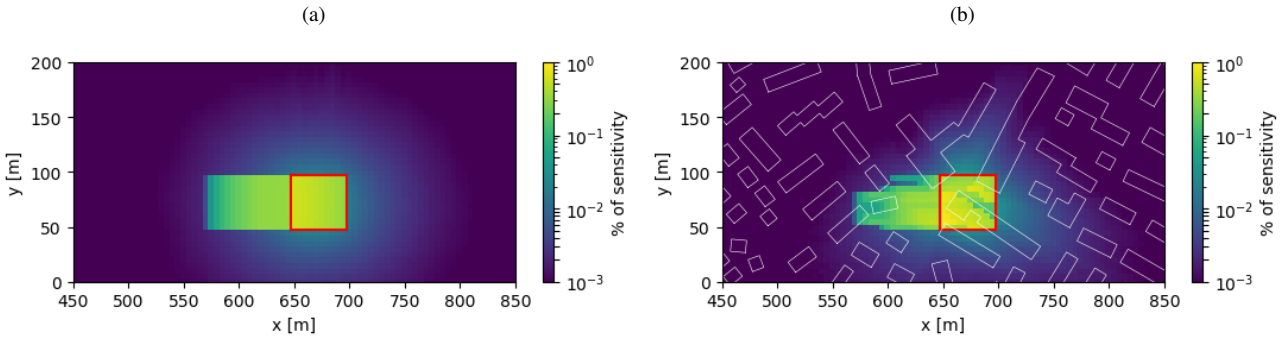

Figure 5. (a) Footprint without buildings. 51.4% of the signal is located outside the ground pixel (i.e. outside the red frame). (b) Footprint with buildings. 52.6% of the instrument sensitivity is located outside the ground pixel. Building contours in white.

Figure 5b presents the same situation but with buildings added to the simulation. Buildings affect the sensitivity both within and outside the ground pixel. The footprint is reduced in the shadows of buildings but may be enhanced over the sunlit sections of streets due to multiple reflections, as seen near the upper right and lower left corners of the ground pixel. In this example, the part of the sensitivity located outside the ground pixel is 52.6%, comparable to the simulation without buildings.

Figure~~S2.6.1~~ S7 in the supplement shows the footprint for the aerosol scenario. The aerosol scattering increases the sensitivity contribution from outside the ground pixel to 55% for both the scenario without and with buildings. The contribution from outside the main optical path is increased to 25% and 32% without and with buildings, respectively, compared to 18% and 24%, when not including aerosols.

The main effect of the 3D optical path of the photons is thus to smear out the sensitivity of a measurement into the direction of the main optical path, which is determined by the viewing and illumination geometry. The presence of buildings further modifies the sensitivity by adding a complex pattern of enhancements and reductions due to ~~shadowing effects~~ the shielding effects of buildings and multiple reflections in street canyons.

3.3 Impact of 3D radiative transfer on NO_2 imaging over a city

In the previous section we have shown how 3D radiative transfer effects and buildings smear out and modify the sensitivity of a single observation. Here we demonstrate how a complete image of NO_2 slant columns is affected by these effects. Note that for simplicity in the following simulations, the ground and building reflectance was set to 0.1.

~~Figure~~

3.3.1 Effects of 3D radiative transfer and buildings on slant column densities

Figure 6 compares total AMFs computed from 1D-layer AMFs (Eq. 2) with total AMFs computed from 3D-box AMFs (Eq. 3) without and with the urban canopy. The corresponding SCDs are presented in the lower row of the figure, which are related to the total AMFs by a division with VCDs shown in ~~Figure~~ Fig. 2c (see Eq. 1 and Eq. 3). In the following we refer to the SCDs

calculated from 1D-layer AMFs as SCD_{1D} and to the SCDs calculated from 3D-box AMFs without and with the urban canopy as SCD_{3D} and SCD_{3D-UC}, respectively.

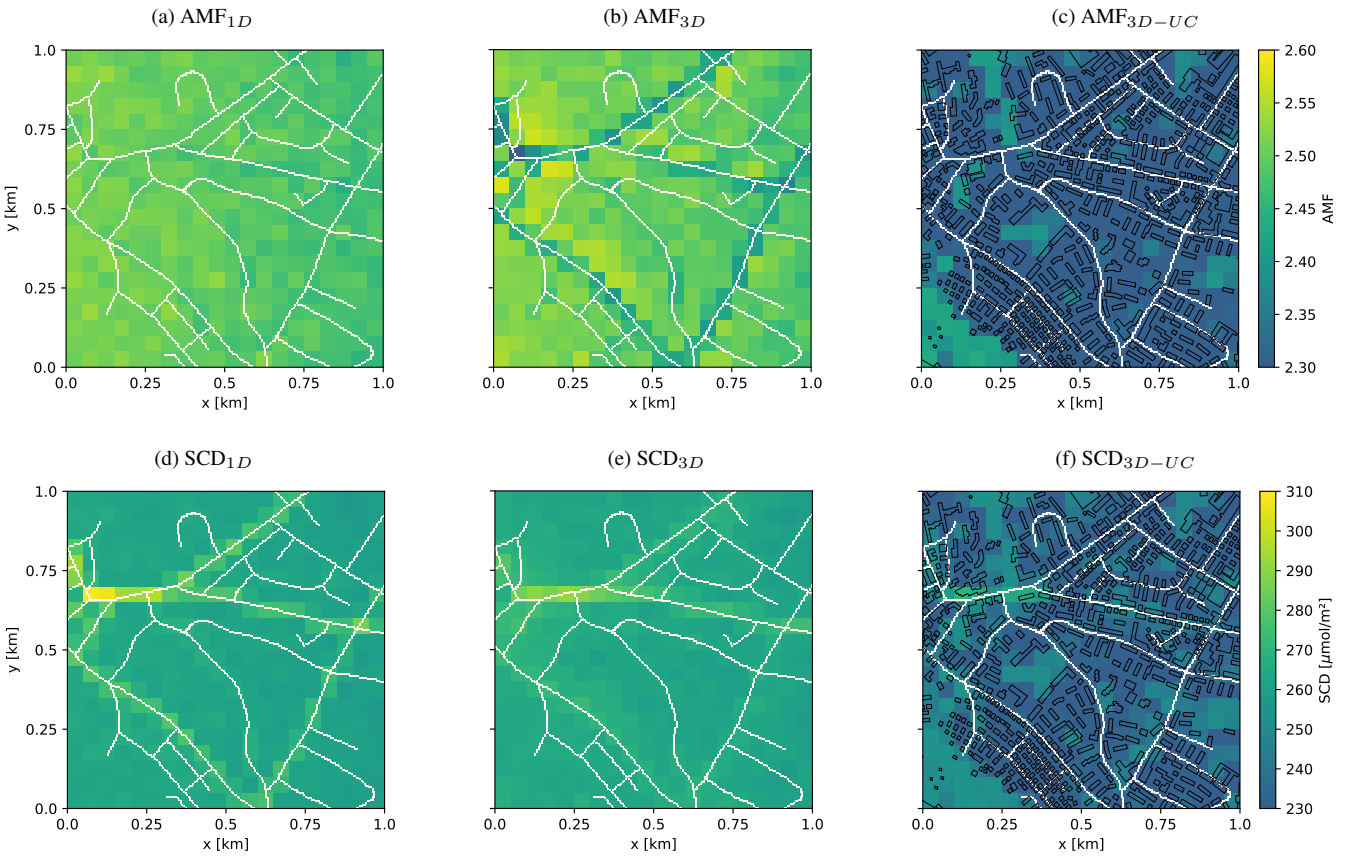

Figure 6. AMFs for a simulation with SAA of 90° with 1D-layer AMFs simulation (a), 3D-box AMFs without (b) and with (c) buildings. The respective SCDs are shown in the lower row (d,e,f). Roads are drawn in white and building contours in black for the simulation with buildings.

AMFs derived from 1D-layer AMFs (~~Figure~~Fig. 6a) are almost horizontally homogeneous. They vary only slightly with the instrument viewing zenith angle and the NO_2 distribution. The contribution of the ~~a-priori~~ a priori NO_2 profile is only significant, when high values collocate with high 1D-layer AMFs values, but as our ~~a-priori~~ a priori NO_2 profiles only ~~differs~~ differ in the lower 100 m, the effect is smaller than the noise of the Monte Carlo simulations (σ_{AMF} = 0.014 and σ_{SCD} = 1.46 µmol m^{-2}). The corresponding SCDs (~~Figure~~Fig. 6d), computed as the sum of the product of the 1D-layer AMFs with the 1D NO_2 profile (see Equ. 2) in ~~Figure~~Fig. 2d show the same pattern as the VCDs with sharply elevated values above roads and a homogeneous background aside. The SCDs are higher than the VCDs because the AMFs are larger than 1.

AMFs calculated with 3D-box AMFs but without buildings (~~Figure~~Fig. 6b) are lower over the roads and slightly larger just aside the roads, because the 3D-optical path crosses neighbouring columns with decreased or increased concentrations,

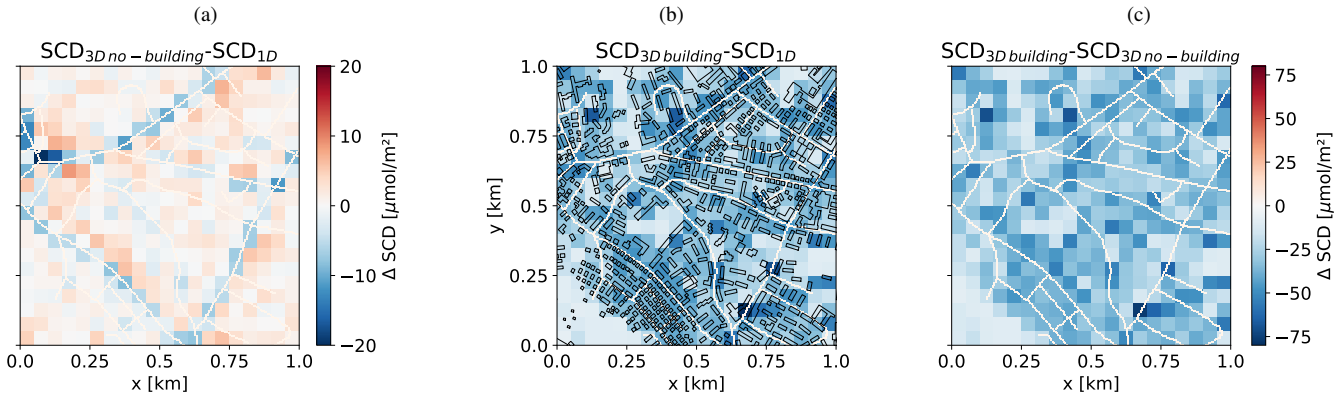

Figure 7. (a) Difference plot between SCDs calculates with 3D-box AMFs and the SCDs calculated with 1D-layer AMFs. (b) Difference plot between SCDs calculated with 3D-box AMFs including the urban canopy and SCDs calculated with 1D-layer AMFs. (c) Difference plot between SCDs calculated with 3D-box AMFs with and without including the urban canopy.

respectively. This results in a spatial smearing of SCDs (~~Figure~~Fig. 6e) mainly in the direction of the main optical path from the sun in the west, to the ground pixel and to the instrument in the east of the center. Far from the roads, the SCDs are homogeneous and more or less identical to the 1D solution. The difference SCD_{3D} minus SCD_{1D} is presented in ~~Figure~~Fig. 7. The smearing effect in the 3D solution is visible as negative differences over the roads and positive differences aside especially on the eastern side of the roads opposite to the sun. As a result, the individual roads show up much less prominently in the SCD_{3D} except for roads parallel to the optical path. The reason for this pattern is illustrated in Fig. 8~~. The~~ , where the main 3D optical path of the photons collected when viewing directly at the road (red path 1 in Fig. 8) misses some of the enhanced NO_2 concentrations in the elevated levels above the road. In contrast, these enhanced NO_2 values are 'seen' by photons collected when viewing to the east of the road (green path 2 in Fig. 8). In the 1D solution, the SCDs are only affected by NO_2 in the vertical column directly above the observed ground pixel.

The mean difference between SCD_{1D} and SCD_{3D} is around 1 $\mu mol\,m^{-2}$ (relative difference of 0.02 %), which suggests that the signal is smeared, but the total amount of measured NO_2 is almost conserved. A small difference is to be expected because of statistical noise from the Monte Carlo method (about 1.3 $\mu mol\,m^{-2}$ for 50000 photons).

AMFs calculated with the 3D-box AMFs module including the urban canopy (~~Figure~~Fig. 6c) also show lower values over roads compared to AMFs calculated with 1D-layer AMFs. In addition, they also show lower values over areas with buildings. As a consequence, the SCDs shown in ~~Figure~~Fig. 6f are lower over regions with many buildings. On average, SCD_{3D-UC} are 12% lower than SCDs without buildings. The standard deviation of the difference between SCD_{3D-UC} and SCD_{3D} is 12.3 $\mu mol\,m^{-2}$ for the whole domain. Not including the urban canopy would therefore underestimate VCDs by 12% and would add a source of noise in the image of about 5% for this particular scenario with rather low buildings. In areas with background NO_2 and no buildings (e.g., lower left region) SCD_{1D}, SCD_{3D} and SCD_{3D-UC} closely agree (Fig. 7c).

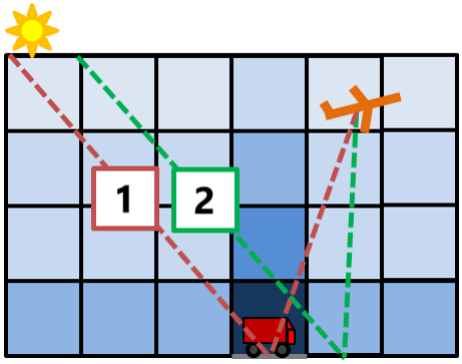

Figure 8. Sketch of ~~the photon path with~~ two main optical paths for an airborne spectrometer pointing at (1) a road in grey and (2) at a pixel aside the road.

The results presented above were obtained for the special situation where viewing and illumination directions were along the same east-west direction. In this case, the smearing effects are most prominent along this axis but relatively small in perpendicular direction. Here, we also analyze the situation where the sun is in the south and thus viewing and illumination directions are perpendicular to each other. As shown in Fig. 9, the results are generally similar but building shadows and correspondingly reduced SCDs are now found to the north instead of the east of the buildings. Furthermore, the SCDs tend to be lower because the main optical path and the corresponding smearing is both N-S (sun to ground pixel) and E-W-oriented (ground pixel to the instrument). The mean difference between SCD_{3D-UC} and SCD_{3D} is 12% and the standard deviation is 13%.

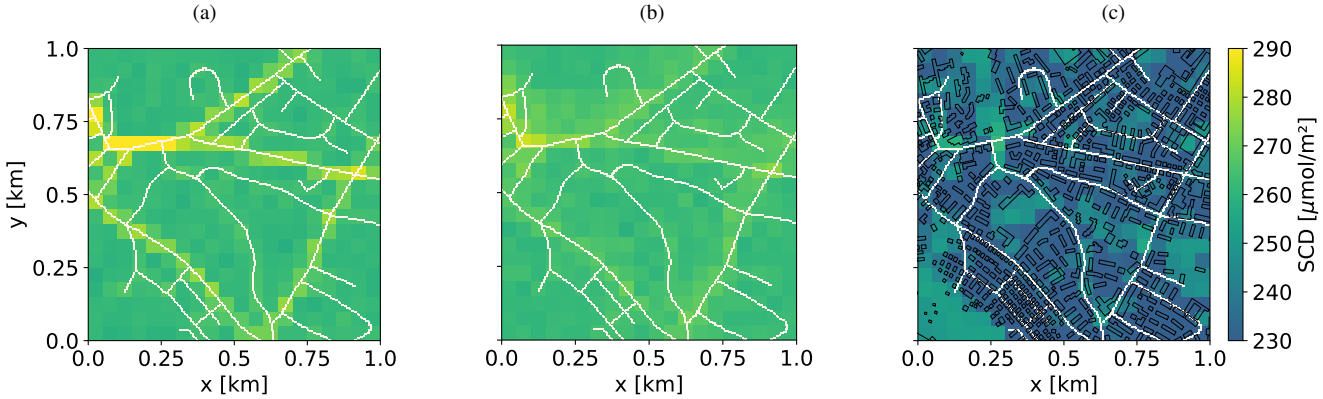

Figure 9. SCDs for simulations with a SAA of 0° with 1D-layer AMFs (a), 3D-box AMFs simulation without (b) and with (c) buildings. The roads are drawn in white and the building contours in black for the simulation with buildings.

3.3.2 3D effects at higher spatial resolution

To investigate the reduced SCDs over buildings observed in the former paragraphs, we analyse the spatial distribution of SCDs within the 50 m x 50 m pixel in more details. For this purpose, we ran additional simulations at higher spatial resolution (5 m x 5 m) for a 100 m x 100 m sub-domain located at x=600 m and y=0 m (lower-left corner of the sub-domain) of the original domain. SCDs were calculated from 3D-box AMFs with and without buildings (Fig. 10a and b).

At this resolution, we can better resolve the spatial distribution of NO_2 and SCDs remain high above roads. Since we can also resolve individual buildings and their shadows, the simulations makes it possible to investigate how buildings reduce SCDs.

At 5 m resolution, we distinguish four types of ground pixels. (1) The ground pixel is on the surface and the geometric path to the sun and the instrument is not obscured by buildings. In this case, the 3D-box AMFs are only affected by buildings through multiple scattering either increasing the AMF when buildings reflect photons towards the ground pixel or reducing the AMF when buildings block photons from reaching the ground pixel. In our example, the effect results in a small but hardly visible reduction of AMFs (see Fig. 10c).

(2) The reflecting point of the geometric path is located on top of a building. The case is similar to the first case, but 3D-box AMFs are smaller, because photons cannot reach the ground. Since we assume that a priori VCDs are fixed regardless of the presence of a building, SCDs are reduced above buildings. However, the effect is very small because only about 3 % of the total VCD is below a 10 m building.

(3) In the third case, the ground pixel is located on the sunlit side of a building, but the direct path to the instrument is blocked by the buildings. Since the VZAs of the simulated instrument are very small, we do not find these cases in our example with rather small buildings.

(4) In the final case, the ground pixel is located in the shadow of the buildings blocking the direct path towards the sun. In this case, photons can only reach the instrument after multiple scattering or simple atmospheric scattering directly into the direction of the instrument, which drastically reduces the 3D-box AMFs near the surface. As a result, SCDs are significantly lower in the shadows of buildings (~~Figure~~ Fig. 10b). For example, SCDs are about 35% lower when increased ground NO_2 concentrations (e.g., road) are located in the shadow of a building.

We can therefore conclude that the reduction of SCDs over buildings (~~Figures~~ Fig. 7c) is mainly caused by the ~~shadow of the building~~ building shielding effect (case 4), while building height has a minor effect on the SCDs (case 2) in our study case with rather small buildings.

3.3.3 The retrieval of vertical column densities

In imaging remote sensing, NO_2 VCDs are retrieved from SCDs using AMFs. Here SCD_{3D-UC} are considered as the "true" SCDs measured by an airborne imaging spectrometer and VCDs were calculated using either 1D-layer AMFs or 3D-box AMFs without buildings (Fig. 11). The VCDs computed with 1D-layer AMFs fails to correct for the spatial smoothing induced by the complex 3D optical path of the photons (Fig. 11b). In additions, the effects of buildings are not corrected resulting in additional

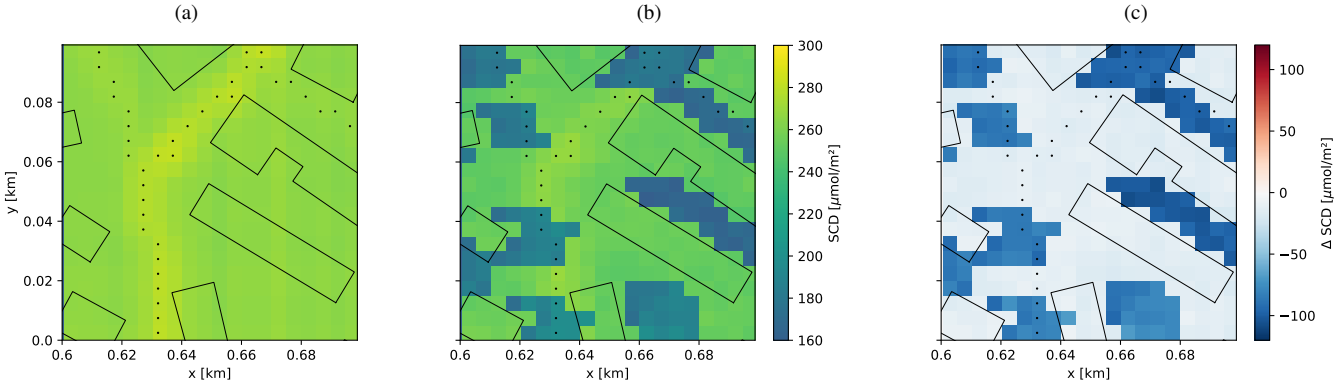

Figure 10. SCDs over a small sub-domain computed from high-resolution 3D-box AMFs simulated without (a) and with (b) buildings and the difference between both (c). In the simulation the sun was located in the west at a SZA of 60°. The albedo of roofs, walls and streets was set to 0.1. Roads are included as black dots and building contours as black lines.

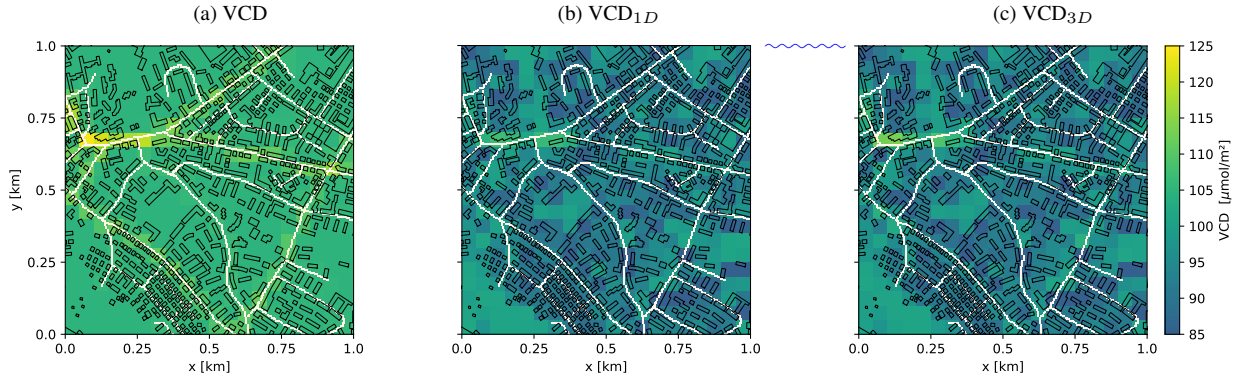

Figure 11. (a) True VCD field and VCDs computed from SCDs using 3D-box AMFs and buildings assuming (b) 1D-layer AMFs and (c) 3D-box AMFs without buildings. The scenario uses a SAA of 90°.

noise introduced by shielding effect of the buildings and significantly lower VCDs with a field average of 90.1 $\mu mol\,m^{-2}$ compared to the 108.4 $\mu mol\,m^{-2}$ of the true VCDs. When VCDs are computed using 3D-box AMFs without buildings, the spatial smearing is corrected but the noise component and lower VCDs (mean: 91.4 $\mu mol\,m^{-2}$) would remain in the retrieved VCDs.

3.4 Application to real observations

The codes developed for this study can also be applied to real observations, for example, to the campaigns conducted with APEX imaging spectrometer. A major challenge is to obtain the required input data. 3D building data are available for many cities, but albedos for ground, roof and walls are generally not available. In addition, realistic 3D NO_2 fields from

a building-resolving dispersion model are required to compute the total AMFs, which requires high-resolution emission inventories and additional model development, because most building-resolving models are not optimized for providing realistic vertical distributions of trace gases or cannot not be applied to a full city at high resolution (Berchet et al., 2017).

To minimize 3D effects when using 1D-layer AMFs, it would be recommendable to obtain the airborne spectrometer measurement around local noon when the SZA is lowest and avoid large viewing zenith angles. However, around noon turbulent atmospheric mixing will be strong and the NO_2 distributions would be smoothed as well.

The computation of 3D-box AMFs with buildings is computationally quite expensive, but still manageable for current airborne campaigns. For example, the computation of the 3D-box AMF field for a single APEX pixel (e.g. on Fig. 6f) takes about 280 s on a single core of our Linux machine (Intel(R) Xeon(R) W-2175 CPU @ 2.50GHz). Processing a full campaign consisting of about 100'000 pixels takes about 23 days using all 14 cores on the system. However, simulating AMFs for an APEX campaign would not require simulation for a 1 km x 1 km domain. Nonetheless, computing 3D-box AMFs is significantly more expensive than computing 1D-layer AMFs and reducing computation time, for example, by finding suitable parametrizations using machine learning, would make it possible to calculate the 3D-box AMFs on smaller hardware, for larger campaigns or to run simulations with more details and at higher spatial resolution.

4 Conclusions

Airborne imaging spectrometers are increasingly used for high-resolution mapping of NO_2 concentrations in cities. The NO_2 maps obtained in this way were usually found to be rather smooth and seemingly inconsistent with the much more rapidly varying near-surface NO_2 concentration fields ~~derived from~~ seen, for example, in city-scale dispersion model simulations. The observed difference may partly be explained by atmospheric mixing more strongly affecting total columns than near-surface concentrations, but could also be caused by complex 3D radiative transfer effects in cities. To study the latter point, we implemented an urban canopy module into the 3D MYSTIC solver of the libRadtran radiative transfer model. We set up a case study for a 1 km x 1 km domain in Zurich, for which 3D-box AMFs and NO_2 slant column densities were computed for a realistic field of NO_2 concentrations.

Our case study shows that the footprint of a single observation is only partly located over the observed ground pixel and that there is a 'tail' in the direction of the main optical path. In the presented simulations with a SZA of 60° and a 50 m x 50 m resolution, about 50% of the sensitivity is located outside the ground pixel for a nearly-nadir viewing instrument. Only a small but not negligible amount of photons are from outside the main optical path, with 19% ~~and~~ for a simulation without aerosols and without buildings and 24% for ~~simulations~~ a simulation without aerosols and ~~without and with buildings, respectively~~with buildings. The effect ~~become~~ becomes more important when aerosols are included with 25% and 32% of the sensitivity located outside the main optical path for scenarios without and with buildings, respectively. The footprint fine structure is further modified with the presence of buildings, but the general shape is conserved.

The 3D radiative transfer simulations show that 3D effects introduce significant spatial smearing of high NO_2 concentrations as for example over roads, which 1D-layer AMFs do not include. This results in increasing SCDs when roads are parallel to

the main optical path and decreasing SCDs otherwise. When buildings are included, NO_2 SCDs are generally lower due to the ~~shadows~~ shielding effect of buildings. The buildings also introduce a variability in the SCD field with a standard deviation of 12.9 $\mu mol\,m^{-2}$ (5.5%) that would show up as additional noise component of airborne imagers. The magnitude is however slightly smaller than the current NO_2 SCD uncertainty (about 20 $\mu mol\,m^{-2}$ for the APEX instrument), but could be noticeable for instruments dedicated to NO_2 mapping that have ~~have~~ lower SCD uncertainties. We also applied 1D-layer and 3D-box AMFs without building to SCDs computed with 3D-box AMFs with buildings showing that 3D radiative transfer simulations are required to correct the smearing effect and that buildings are required to avoid an underestimation of the VCDs.

Generalizing our results to others cities is challenging, because many relevant parameters such as building shapes, surface reflectances and a priori NO_2 distribution vary strongly between different cities. In our case study, we used a surface reflectance of 0.1, which is a realistic value for Zurich but not necessarily for other cities. In general, a higher surface reflectance of the observed ground pixel implies less atmospheric scattering and a higher sensitivity of the instrument to the main optical path and higher albedo of neighbouring pixels increases the sensitivity to this neighbouring pixel. In this study, the simulations were conducted at 490 nm, which corresponds to the center of the fitting window used for NO_2 retrieval from the APEX airborne spectrometer. At shorter wavelength, used by other instruments, scattering increases, which decreases the instrument sensitivity to the main optical path. The footprint simulated with a wavelength of 420 nm (without buildings) shows the increase in scattering and the sensitivity to neighbouring pixels, as 56% of the sensitivity is located outside of the ground pixel.

In conclusion, our case study demonstrates that 3D effects explain the smooth NO_2 field observed by airborne imaging spectrometers, at least partly. Atmospheric mixing can still result in additional smoothing that has not been studied here. Furthermore, buildings reduce SCDs due to ~~shadows~~ light shielding effect of buildings and add an additional noise component that is difficult to generalize due to the complexity and the heterogeneity of the buildings. The smearing in sun direction can result in features in the maps that are difficult to interpret when the sun position is not known. 3D radiative transfer effects therefore need to be considered when studying NO_2 maps obtained from airborne imagers and might become relevant with future NO_2 satellite instruments that measure NO_2 at spatial resolutions down to 2 km.

Code availability. The libRadtran package including the 1D version of MYSTIC is freely available on www.libradtran.org, the 3D MYSTIC code is available upon request to Claudia Emde (claudia.emde@lmu.de). The Python script used to create a triangular mesh from ESRI shapefiles will be available on Gitlab after the final revision of the manuscript and the other used codes are available upon request to the corresponding author.

Data availability. The data is available upon request to Marc Schwärzel (marc.schwaerzel@empa.ch) for the discussion paper and will be made available on https://zenodo.org for the final revised paper.

Author contributions. MS designed and implemented the urban canopy module, designed and simulated the 3D scenarios and wrote the manuscript with input from all co-authors. FJ designed and implemented the urban canopy module together with MS and CE. DB, BB and AB provided critical feedback to the study and reviewed the manuscript, GK supervised the study, designed together with MS the case studies and reviewed the manuscript.

Competing interests. The authors declare that they have no conflict of interest.

Acknowledgements. This study was conducted as part of the HighNOCS project funded by the Swiss National Science Foundation (SNSF) under project number 172533. We obtained building data from the Swiss Federal Office of Topography (swisstopo) and the traffic emission inventories from the City of Zurich.

References

Berchet, A., Zink, K., Muller, C., Oettl, D., Brunner, J., Emmenegger, L., and Brunner, D.: A cost-effective method for simulating city-wide air flow and pollutant dispersion at building resolving scale, Atmospheric Environment, 158, 181–196, https://doi.org/https://doi.org/10.1016/j.atmosenv.2017.03.030, 2017.

Bär, P.: Luftbilanz 2016: Resultate der flächendeckenden Messkampagne, 2016.

Cracknell, A. P. and Varotsos, C.: Remote sensing and atmospheric ozone: Human activities versus natural variability, Springer Science & Business Media, 2012.

de Goeij, B. T. G., Otter, G. C. J., van Wakeren, J. M. O., Veefkind, J. P., Vlemmix, T., Ge, X., Levelt, P. F., Dirks, B. P. F., Toet, P. M., van der Wal, L. F., and Jansen, R.: First aircraft test results of a compact, low cost hyperspectral imager for earth observation from space, in: International Conference on Space Optics — ICSO 2016, edited by Cugny, B., Karafolas, N., and Sodnik, Z., vol. 10562, pp. 465 – 475, International Society for Optics and Photonics, SPIE, https://doi.org/10.1117/12.2296068, https://doi.org/10.1117/12.2296068, 2017.

de Graaf, M., Sihler, H., Tilstra, L. G., and Stammes, P.: How big is an OMI pixel?, Atmos. Meas. Tech., 9, 3607–3618, https://doi.org/10.5194/amt-9-3607-2016, http://www.atmos-meas-tech.net/9/3607/2016/, 2016.

Deutschmann, T., Beirle, S., Frieß, U., Grzegorski, M., Kern, C., Kritten, L., Platt, U., Prados-Román, C., Puķıˉte, J., Wagner, T., Werner, B., and Pfeilsticker, K.: The Monte Carlo atmospheric radiative transfer model McArtim: Introduction and validation of Jacobians and 3D features, Journal of Quantitative Spectroscopy and Radiative Transfer, 112, 1119–1137, https://doi.org/10.1016/j.jqsrt.2010.12.009, http://www.sciencedirect.com/science/article/pii/S0022407310004668, 2011.

Emde, C. and Mayer, B.: Simulation of solar radiation during a total eclipse: a challenge for radiative transfer, Atmospheric Chemistry and Physics, 7, 2259–2270, 2007.

Emde, C., Buras-Schnell, R., Kylling, A., Mayer, B., Gasteiger, J., Hamann, U., Kylling, J., Richter, B., Pause, C., Dowling, T., and Bugliaro, L.: The libRadtran software package for radiative transfer calculations (version 2.0.1), Geoscientific Model Development, 9, 1647–1672, https://doi.org/10.5194/gmd-9-1647-2016, 2016.

Gastellu-Etchegorry, J.-P., Yin, T., Lauret, N., Cajgfinger, T., Gregoire, T., Grau, E., Feret, J.-B., Lopes, M., Guilleux, J., Dedieu, G., Malenovský, Z., Cook, D. B., Morton, D., Rubio, J., Durrieu, S., Cazanave, G., Martin, E., and Ristorcelli, T.: Discrete Anisotropic Radiative Transfer (DART 5) for Modeling Airborne and Satellite Spectroradiometer and LIDAR Acquisitions of Natural and Urban Landscapes, Remote Sensing, 7, https://doi.org/10.3390/rs70201667, 2015.

Kuhlmann, G., Hueni, A., Damm, A., and Brunner, D.: An Algorithm for In-Flight Spectral Calibration of Imaging Spectrometers, Remote Sensing, 8, 1017, https://doi.org/10.3390/rs8121017, 2016.

Kuhlmann, G., Berchet, A., and Brunner, D.: High-resolution remote sensing and modelling of NO2 air pollution over the city of Zurich, in: 10th EARSeL SIG Imaging Spectroscopy Workshop 2017, Zurich, Switzerland, https://doi.org/10.5281/zenodo.5220909, 2017.

Lyapustin, A. and Kaufman, Y.: Role of adjacency effect in the remote sensing of aerosol, Journal of Geophysical Research: Atmospheres, 106, 11 909–11 916, 2001.

Marchuk, G., Mikhailov, G., Nazaraliev, M., Dacbinjan, R., Kargin, B., and Elepov, B.: Monte Carlo methods in atmospheric optics, Berlin, Germany, 1980.

Massie, S. T., Sebastian Schmidt, K., Eldering, A., and Crisp, D.: Observational evidence of 3-D cloud effects in OCO-2 CO2 retrievals, Journal of Geophysical Research: Atmospheres, 122, 7064–7085, https://doi.org/https://doi.org/10.1002/2016JD026111, https://agupubs.onlinelibrary.wiley.com/doi/abs/10.1002/2016JD026111, 2017.

Mayer, B.: Radiative transfer in the cloudy atmosphere, in: EPJ Web of Conferences, vol. 1, pp. 75–99, EDP Sciences, 2009.

Mayer, B. and Kylling, A.: Technical note: The libRadtran software package for radiative transfer calculations - description and examples of use, Atmospheric Chemistry and Physics, 5, 1855–1877, 2005.

Merlaud, A., Constantin, D., Mingireanu, F., Mocanu, I., Fayt, C., Maes, J., Murariu, G., Voiculescu, M., Georgescu, L., and Van Roozendael, M.: Small whiskbroom imager for atmospheric composition monitoring (SWING) from an unmanned aerial vehicle (UAV), in: Proceedings of the 21st ESA Symposium on European Rocket & Balloon Programmes and related Research, Thun, Switzerland, pp. 9–13, 2013.

Minomura, M., KUzE, H., and Takeuchi, N.: Adjacency effect in the atmospheric correction of satellite remote sensing data: Evaluation of the influence of aerosol extinction profiles, Optical review, 8, 133–141, 2001.

Mussetti, G., Brunner, D., Henne, S., Allegrini, J., Krayenhoff, E. S., Schubert, S., Feigenwinter, C., Vogt, R., Wicki, A., and Carmeliet, J.: COSMO-BEP-Tree v1. 0: a coupled urban climate model with explicit representation of street trees, Geoscientific Model Development, 13, 1685–1710, 2020.

Nowlan, C. R., Liu, X., Leitch, J. W., Chance, K., González Abad, G., Liu, C., Zoogman, P., Cole, J., Delker, T., Good, W., Murcray, F., Ruppert, L., Soo, D., Follette-Cook, M. B., Janz, S. J., Kowalewski, M. G., Loughner, C. P., Pickering, K. E., Herman, J. R., Beaver, M. R., Long, R. W., Szykman, J. J., Judd, L. M., Kelley, P., Luke, W. T., Ren, X., and Al-Saadi, J. A.: Nitrogen dioxide observations from the Geostationary Trace gas and Aerosol Sensor Optimization (GeoTASO) airborne instrument: Retrieval algorithm and measurements during DISCOVER-AQ Texas 2013, Atmospheric Measurement Techniques, 9, 2647–2668, https://doi.org/10.5194/amt-9-2647-2016, http://www.atmos-meas-tech.net/9/2647/2016/, 2016.

Palmer, P. I., Jacob, D. J., Chance, K., Martin, A. V., Robert J., D., Kurosu, T. P., Bey, I., Yantosca, R., Fiore, A., and Li, Q.: Air mass factor formulation for spectroscopic measurements from satellites: Application to formaldehyde retrievals from the global ozone monitoring experiment, Journal of Geophysical Research, pp. 14–539, 2001.

Popp, C., Brunner, D., Damm, A., Van Roozendael, M., Fayt, C., and Buchmann, B.: High-resolution NO2 remote sensing from the Airborne Prism EXperiment (APEX) imaging spectrometer, Atmospheric Measurement Techniques, 5, 2211–2225, https://doi.org/10.5194/amt-5-2211-2012, http://www.atmos-meas-tech.net/5/2211/2012/, 2012.

Richter, R.: A fast atmospheric correction algorithm applied to Landsat TM images, TitleREMOTE SENSING, 11, 159–166, 1990.

Schaepman, M. E., Jehle, M., Hueni, A., D'Odorico, P., Damm, A., Weyermann, J., Schneider, F. D., Laurent, V., Popp, C., Seidel, F. C., Lenhard, K., Gege, P., Küchler, C., Brazile, J., Kohler, P., De Vos, L., Meuleman, K., Meynart, R., Schläpfer, D., Kneubühler, M., and Itten, K. I.: Advanced radiometry measurements and Earth science applications with the Airborne Prism Experiment (APEX), Remote Sensing of Environment, 158, 207–219, https://doi.org/10.1016/j.rse.2014.11.014, http://www.sciencedirect.com/science/article/pii/S0034425714004568, 2015.

Schönhardt, A., Altube, P., Gerilowski, K., Krautwurst, S., Hartmann, J., Meier, A., Richter, A., and Burrows, J. P.: A wide field-of-view imaging DOAS instrument for two-dimensional trace gas mapping from aircraft, Atmospheric Measurement Techniques, pp. 5113–5131, 2015.

Schwaerzel, M., Emde, C., Brunner, D., Morales, R., Wagner, T., Berne, A., Buchmann, B., and Kuhlmann, G.: Three-dimensional radiative transfer effects on airborne and ground-based trace gas remote sensing, Atmospheric Measurement Techniques, 13, 4277–4293, https://doi.org/https://doi.org/10.5194/amt-13-4277-2020, 2020.

Tack, F., Merlaud, A., Iordache, M. D., Danckaert, T., Yu, H., Fayt, C., Meuleman, K., Deutsch, F., Fierens, F., and Van Roozendael, M.: High resolution mapping of the NO2 spatial distribution over Belgian urban areas based on airborne APEX remote sensing, Atmos. Meas. Tech. Discuss., 2017, 1–52, https://doi.org/10.5194/amt-2016-400, 2017.

Tack, F., Merlaud, A., Meier, A. C., Vlemmix, T., Ruhtz, T., Iordache, M.-D., Ge, X., Van Der Wal, L., Schuettemeyer, D., Ardelean, M., et al.: Intercomparison of four airborne imaging DOAS systems for tropospheric NO 2 mapping–the AROMAPEX campaign, Atmospheric Measurement Techniques, 12, 211, 2019.

Villefranque, N., Fournier, R., Couvreux, F., Blanco, S., Cornet, C., Eymet, V., Forest, V., and Tregan, J.-M.: A Path-Tracing Monte Carlo Library for 3-D Radiative Transfer in Highly Resolved Cloudy Atmospheres, Journal of Advances in Modeling Earth Systems, 11, 2449–2473, https://doi.org/https://doi.org/10.1029/2018MS001602, https://agupubs.onlinelibrary.wiley.com/doi/abs/10.1029/2018MS001602, 2019.

Vlemmix, T., Ge, X. ., de Goeij, B. T. G., van der Wal, L. F., Otter, G. C. J., Stammes, P., Wang, P., Merlaud, A., Schüttemeyer, D., Meier, A. C., Veefkind, J. P., and Levelt, P. F.: Retrieval of tropospheric NO_2 columns over Berlin from high-resolution airborne observations with the spectrolite breadboard instrument, Atmospheric Measurement Techniques Discussions, 2017, 1–34, https://doi.org/10.5194/amt-2017-257, https://amt.copernicus.org/preprints/amt-2017-257/, 2017.